Journal of Anatomy

J. Anat. (2016) **228**, pp746–756 doi: 10.1111/joa.12437

Global deletion of *Panx3* produces multiple phenotypic effects in mouse humeri and femora

Deidre Caskenette,[1] Silvia Penuela,[1] Vanessa Lee,[1] Kevin Barr,[1] Frank Beier,[2,3] Dale W. Laird[1,2] and Katherine E. Willmore[1]

[1]*Department of Anatomy and Cell Biology, University of Western Ontario, London, ON, Canada*
[2]*Department of Physiology and Pharmacology, University of Western Ontario, London, ON, Canada*
[3]*Children's Health Research Institute, London, ON, Canada*

Abstract

Pannexins form single-membrane channels that allow passage of small molecules between the intracellular and extracellular compartments. Of the three pannexin family members, Pannexin3 (Panx3) is the least studied but is highly expressed in skeletal tissues and is thought to play a role in the regulation of chondrocyte and osteoblast proliferation and differentiation. The purpose of our study is to closely examine the *in vivo* effects of Panx3 ablation on long bone morphology using micro-computed tomography. Using Panx3 knockout (KO) and wildtype (WT) adult mice, we measured and compared aspects of phenotypic shape, bone mineral density (BMD), cross-sectional geometric properties of right femora and humeri, and lean mass. We found that KO mice have absolutely and relatively shorter diaphyseal shafts compared with WT mice, and relatively larger areas of muscle attachment sites. No differences in BMD or lean mass were found between WT and KO mice. Interestingly, KO mice had more robust femora and humeri compared with WT mice when assessed in cross-section at the midshaft. Our results clearly show that Panx3 ablation produces phenotypic effects in mouse femora and humeri, and support the premise that Panx3 has a role in regulating long bone growth and development.

Key words: bone mineral density; cross-sectional geometry; geometric morphometrics; long bones; mice; Pannexin3.

Introduction

Members of the pannexin family of proteins form single-membrane channels that connect the intracellular cytosol of cells with the extracellular environment (Penuela et al. 2007, 2013; Sosinsky et al. 2011). These channels facilitate the movement of small molecules such as ATP, resulting in the induction of multiple signaling pathways (Bao et al. 2004; Scemes et al. 2009; Ishikawa et al. 2011; Penuela et al. 2014). The three-member pannexin family consists of Panx1, Panx2 and Panx3 (Panchin et al. 2000). Panx1 is the most extensively studied and seemingly has the widest expression of the pannexin members (Baranova et al. 2004). Panx2 is more abundant in the central nervous system (Baranova et al. 2004) but has also been reported in other tissues (Le Vasseur et al. 2014). Panx3 has been shown to be expressed in the epidermis (Baranova et al. 2004; Penuela et al. 2008), kidney arterioles (Bond & Naus, 2014), Leydig cells, epididymis, efferent ducts (Turmel et al. 2011), mammary glands (Bond et al. 2011) and skeletal muscle (Langlois et al. 2014). Importantly, Panx3 is probably most highly expressed in skeletal tissues (Baranova et al. 2004; Penuela et al. 2007; Bond et al. 2011; Ishikawa et al. 2011). Through immunohistochemistry, Panx3 has been found to occur in bones derived from both endochondral and intramembranous ossification (Wang et al. 2009; Iwamoto et al. 2010; Bond et al. 2011; Ishikawa et al. 2011; Oh et al. 2015). Thus, Panx3 likely plays a functional role in the regulation of developmental processes in all bones.

In endochondral ossification, a hyaline cartilage template is formed and then replaced by bone (Ross & Pawlina, 2011). The process of endochondral ossification begins with the aggregation of mesenchymal stem cells. Cells in the center of the aggregate differentiate into chondrocytes and form the growth plate, whereas those cells at the periphery of the aggregate form the perichondrium (Long & Ornitz, 2013). In the developing growth plate, chondrocytes organize into discrete zones according to their stage of matura-

Correspondence
Katherine E. Willmore, Department of Anatomy and Cell Biology, Medical Sciences Bldg, Rm 488 University of Western Ontario, London, ON, Canada, N6A 5C1. T: + 1 519 6612111 ext. 88079; E: kwillmo2@uwo.ca

Accepted for publication *5 December 2015*
Article published online *7 January 2016*

tion. Moving towards the diaphysis from the growth plate, the zones of proliferative, maturing and hypertrophic chondrocytes are evident (White & Wallis, 2001; Kronenberg, 2003; Ross & Pawlina, 2011). The matrix secreted by hypertrophic chondrocytes calcifies and through partial resorption of this calcified matrix, spicules of calcified cartilage are formed that serve as a scaffold for osteoblasts to deposit new bone (Ross & Pawlina, 2011). Until recently, the established view of the ossification process is that hypertrophic chondrocytes within the calcified matrix undergo apoptosis and are replaced by invading osteoblast precursors (Kronenberg, 2003). However, there is mounting evidence that hypertrophic chondrocytes within the calcified matrix can differentiate into osteoblasts (Hammond & Schulte-Merker, 2009; Pest & Beier, 2014; Tsang et al. 2015). Regardless, the spatial and temporal control of chondrocyte proliferation and differentiation is crucial for endochondral ossification and we hypothesize that Panx3 plays an important role in one or more of these critical developmental processes.

In endochondral ossification, Panx3 is first expressed by chondrocytes in the pre-hypertrophic zone of the developing growth plate (Iwamoto et al. 2010; Ishikawa et al. 2011; Oh et al. 2015). Here, Panx3 oligomerizes to form channels prior to transport to the plasma membrane where it can act to release ATP (as well as potentially other small molecules) from the interior of the cell to the extracellular space. This release of ATP is thought to lead to inhibition of the PTH/PTHrP signaling pathway that drives chondrocyte proliferation (Iwamoto et al. 2010). Additionally, the release of ATP results in reduced intracellular cAMP levels, thus inhibiting PKA/CREB signaling, which has the effect of downregulating proliferation (Iwamoto et al. 2010; Oh et al. 2015). Panx3 expression also promotes the differentiation of chondrocytes from a proliferative to post-mitotic state (Iwamoto et al. 2010). The role of Panx3 in chondrocyte proliferation and differentiation at the growth plate indicates that it is likely involved in the regulation of endochondral ossification and therefore, importantly for our study, in the regulation of long bone growth and development.

Panx3 is also expressed in osteoprogenitor cells and osteoblasts (Iwamoto et al. 2010; Ishikawa et al. 2011). An *in vitro* study by Ishikawa et al. (2011) found that in cells that overexpress Panx3, osteoblast marker genes were upregulated and mineralization was increased. Recent *in vivo* results support *in vitro* findings, as mineralization of bones derived from both endochondral and intramembranous ossification was delayed in mice lacking Panx3 (Oh et al. 2015). Conversely, in cells where Panx3 expression had been inhibited, the opposite pattern was observed, indicating a role for Panx3 in promoting osteoblast differentiation. From studies of C2C12 cells and primary calvarial cells, Ishikawa et al. (2011) suggested that Panx3 promotes osteoblast differentiation by acting as an endoplasmic reticulum Ca^{2+} channel. Panx3 has also been shown to play a key role in inhibiting osteoprogenitor proliferation and promoting cell cycle exit (Ishikawa et al. 2014). Therefore, through its role in regulating osteoprogenitor and osteoblast proliferation and differentiation, it is likely that Panx3 influences both endochondral and intramembranous ossification.

The current understanding of the role of Panx3 in bone biology comes mainly from *in vitro* and *ex vivo* studies, but there are a couple of recently published *in vivo* studies. The first of these studies used our global as well as a cartilage-specific Panx3 knockout (KO) mouse model. Unexpectedly, our group found no gross difference in femur length between KO and wildtype (WT) mice (Moon et al. 2015). The second paper by Oh et al. (2015) used a different global Panx3-null mouse as well as Panx3 knockdown morpholinos in zebrafish to study the effects of Panx3 in bone development. This latter study supports the premise that Panx3 plays a key role in chondrocyte and osteoblast proliferation and differentiation.

Here we provide a detailed phenotypic assessment of femora and humeri from Panx3-ablated mice using data collected from micro-computed tomography (μCT) images. Using geometric morphometric analyses on three-dimensional anatomical landmark data, we found that KO mice had absolutely shorter femoral and humeral diaphyses, and relatively larger muscle attachment sites than WT mice. Contrary to our prediction, bone mineral density analysis revealed no differences between mouse groups for either femora or humeri. Comparisons of cross-sectional geometric properties of long bones indicate that KO mice have more robust femora and humeri at the midshaft, and are predicted to better resist compressional and torsional forces than WT mice. Additionally, we found no significant differences in lean mass, body weight and lean mass standardized by body weight between KO and WT mice. Overall, our phenotypic analyses serve to elucidate the role of Panx3 in long bone formation.

Materials and methods

Animals

Our sample comprises 10 WT and 10 Panx3 global KO mice aged 2 or 3 months. The Panx3 KO mice were generated on a C57BL/6N mouse background using the Cre/loxP recombinase system (Moon et al. 2015). Absence of Panx3 in the knockout mice was verified using PCR genotyping and Western blots. Details of the generation and verification of the Panx3 KO mouse are described in a recent paper by Moon et al. (2015). The WT mice used in our study were C57BL/6N non-littermate controls. Mice were housed in standard cages, maintained on a 12-h light/dark cycle, with *ad libitum* access to water and standard mouse chow (2018 Tekland Global 18% Protein Diet; Harlan Laboratories, Indianapolis, IN, USA). All aspects of our study were conducted in accordance with the policies and guidelines of the Canadian Council on Animal Care and were approved by the Animal Use Subcommittee of the University of Western Ontario, London, ON, Canada.

Micro-computed tomography

We obtained high resolution μCT whole body images of live mice using the eXplore speCZT μCT scanner (GE Healthcare, Waukesha, WI, USA) at Robarts Research Institute (London, ON, Canada). We anesthetized the mice through face cone-administered isofluorane (Forane, catalog #CA2L9100; Baxter Corporation, Mississauga, ON, Canada) and used *in vivo* scanning techniques following Granton et al. (2010). In one rotation of the beam, 900 views were obtained at 0.40 intervals over a 5-min period (16 ms exposure). Images were acquired at an isotropic voxel size of 50 μm and reconstructed into 3D volumes at 100 μm to reduce noise associated with breathing. Two separate scans were required to capture the whole mouse. The two scans were then digitally 'stitched' together to render a full 3D volume of the entire mouse. In a separate scan, we imaged calibration samples of water and a synthetic cortical-bone mimicking epoxy with a bone mineral equivalent of 1100 mg cm^{-3} (SB3, Gamex, Middleton, WI, USA) to ensure accurate calibration of CT greyscale intensities in Hounsfield units (HU). Through manual segmentation, we isolated right femora and humeri from reconstructed whole body images using MicroView (GE Healthcare Biosciences).

Landmark data collection

Three-dimensional landmark coordinate data were used to compare long bone morphology between WT and Panx3 KO mice. Landmark data are superior to traditional measures of shape such as scalar measures of length, as they preserve relationships among data points and allow us to quantify and compare the geometry of form (Baab et al. 2012). From 3D reconstructions of μCT data, one of us (D.C.) digitized landmark coordinate data using eTDIPS, a multidimensional volume visualization and analysis software, co-developed by the National Institutes of Health and the National University of Singapore. We recorded 14 landmarks for each right femur (n = 18), and 12 landmarks for each right humerus (n = 20). Femora from two mice (one WT and one KO) were not used due to movement artifacts. Figure 1 illustrates both femoral and humeral landmark positions and Table 1 provides an anatomical description of each landmark. Features along the articulating joint surfaces could not be landmarked as we were unable to precisely separate the bones at the joints through manual segmentation. To assess the repeatability of the chosen landmarks, we digitized four bones four times. Points that could be repeated within 0.05 mm of error were deemed acceptable (Frelat et al. 2012). We chose landmarks for our analyses based on accuracy of digitizing and to provide as complete coverage of the femur and humerus as possible. We further minimized measurement error by landmarking each bone twice, checking for gross errors and using the average of the two data collection trials in analyses.

Shape analyses

We use geometric morphometric analyses to quantify and compare three-dimensional shape features between KO and WT mouse femora and humeri. Geometric morphometric analyses use geometric data (landmarks) instead of traditional measurements such as distances. These analyses are advantageous for studies of phenotypic shape, as they preserve the original geometric form among landmarks and they provide a powerful statistical means to quantify and compare shape. These measures also enable the user to include or exclude allometric effects on shape and detect subtle differences in shape that might otherwise be overlooked.

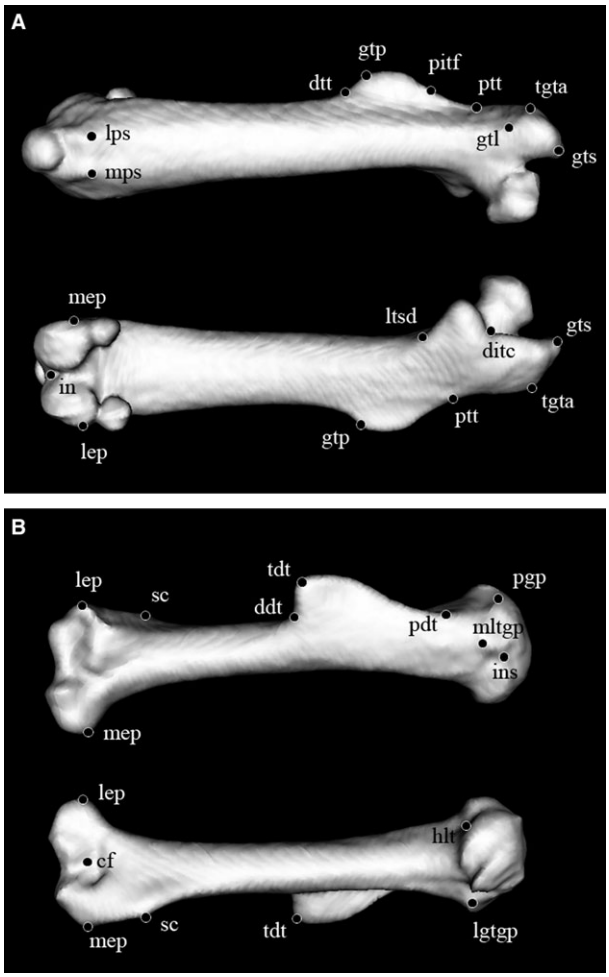

Fig. 1 Three-dimensional landmarks collected from μCT scans of right femora (A) and right humeri (B). (A) The 14 landmarks collected from femora shown in rostral (above) and caudal (below) views. (B) The 12 landmarks collected from humeri shown in rostral (above) and caudal (below) views. See Table 1 for an anatomical description of the landmarks used.

To analyze overall long bone shape differences between groups, we used principal components analysis (PCA) on Procrustes-transformed data, and to determine localized differences in shape between WT and KO mice we used Euclidean distance matrix analysis (EDMA) (Lele & Richtsmeier, 1991, 2001). Principal components analysis is a data reduction technique that reduces the dimensionality of the dataset. We used PCA as it enables visualization of shape changes along axes (principal components) that account for the greatest shape variation among individuals. EDMA estimates localized differences between mouse groups by statistically comparing all unique pairwise distances between landmarks (pairwise distances: femur 91, humerus 66). A non-parametric bootstrap procedure (10 000 resamples) is used to calculate confidence intervals for each distance. Thus, both of these analyses incorporate information from all of the 3D landmarks and are appropriate for small samples.

We performed PCA on Procrustes-transformed coordinates to visualize overall shape changes between mouse groups using the

Table 1 List of femoral and humeral landmarks used in this study (see Fig. 1) including their abbreviations and a brief anatomical description.

Femoral landmarks	
Abbreviation	Description of landmark location
in	Intercondylar fossa
gts	Tip of greater trochanter
gtp	Tip of third trochanter
ditc	Distal intertrochanteric crest
pitf	Point of greatest curvature of longest arm of third trochanter
gtl	Anterior corner of greater trochanter
ptt	Proximal end of third trochanter
dtt	Distal end of third trochanter
ltsd	Distal end under lesser trochanter on shaft
tgta	Line where third trochanter meets greater trochanter
lep	Lateral epicondyle
lps	Lateral aspect of superior tip of patellar articular surface
mps	Medial aspect of superior tip of patellar articular surface
mep	Medial epicondyle

Humeral landmarks	
Abbreviation	Description of landmark location
ins	Superior point on proximal growth plate between greater and lesser tubercle
pgp	Superior point on proximal growth plate lateral view
mltgp	Medial side greater tubercle meets proximal growth plate
lgtgp	Lateral side tubercle meets growth plate
hlt	Between head of humerus and lesser tubercle at level of growth plate
pdt	Proximal deltoid tuberosity
tdt	Tip of deltoid tuberosity
ddt	Distal deltoid tuberosity
lep	Lateral epicondyle
sc	Supinator crest (most lateral point)
cf	Olecranon fossa
mep	Medial epicondyle

program MORPHOJ v. 1.06d (Klingenberg, 2011). We used Procrustes-transformed raw landmark coordinates to remove the effects of scale, translation and rotation (Gower, 1975; Rohlf & Slice, 1990; Bookstein, 1991). To account for the potential effects of age at time of scanning (2 or 3 months), we used a multivariate regression of Procrustes coordinates on age. Age accounted for 6% ($P < 0.01$) of the total variation in femora and 14% ($P < 0.01$) of the total variation in humeri. Therefore, we used residuals from these regressions for subsequent analyses of Procrustes data to remove the effects of age.

While Procrustes transformation removes the effect of scale, it does not remove the allometric component of shape. Thus, we also performed a multivariate regression of the Procrustes coordinates on centroid size (the square root of the sum of the squared distances of the set of landmarks from their centroid). We performed PCA analysis on both the original Procrustes coordinate data and residual data from the regression of Procrustes data on centroid size. Both sets of data offer complimentary information on shape. While the allometric component of shape is biologically important, its large effect on shape variation can overwhelm more subtle aspects of shape variation (Porto et al. 2013).

We measured localized differences in shape using EDMA using both FORM and SHAPE modules (Lele & Richtsmeier, 1991, 2001). The FORM analysis uses the raw inter-landmark distances to compute differences. The SHAPE analysis uses inter-landmark distances that have been scaled by the geometric mean (*n*th root of the product of all inter-landmark distances within a group) to compute differences in like linear distances. Thus, as with the PCA analyses, we measured localized shape differences with (FORM) and without (SHAPE) the allometric component of shape. A small number of inter-landmark distances were significantly correlated with age at time of scanning (10 of 91 distances for the femur, and 9 of 66 distances for the humerus). We excluded these distances from analyses.

Bone mineral density

We calculated bone mineral density (BMD) as the ratio of the average HU value of the bone region of interest to the measured HU value of the SB3 (synthetic cortical-bone mimicking epoxy) calibrator using a script written for MICROVIEW software (Beaucage et al. 2014). Again, we tested for the effect of age on BMD and the correlation was insignificant. To determine the difference in BMD between groups we used Welch's two-sample *t*-test in R statistical computing environment.

Cross-sectional geometric properties

We aligned the segmented bones in MICROVIEW and obtained 100-μm-thick cross-sections orthogonal to the long axis of each bone. Due to movement artifact, we excluded two WT and two KO mice from cross-sectional geometric analyses. We obtained cross-sections at 50% of bone length for the femur and at 40% of bone length measured from the distal end for the humerus (to avoid the deltoid tuberosity). Similar cross-sectional locations have been used in previous studies assessing long bone diaphyseal mechanical performance (Ruff, 2008).

We imported cross-sectional images into IMAGEJ (NIH) and set a consistent density threshold to represent bone. We calculated bone cross-sectional measurements including cortical bone area (CA), total subperiosteal area (TA), second moments of area (I_{max} and I_{min}), and second polar moment of area (J) using MomentMacro, a plugin for IMAGEJ. We calculated the percent cortical area (%CA) and I_{max}/I_{min} from the cross-sectional properties obtained using MomentMacro. We controlled for body size variation by standardizing the cross-sectional geometric measurements. We used the following standardization formulas: J/(body mass $\times$ bone length^2); CA/body mass; TA/body mass; I_{max}/(body mass $\times$ length^2); I_{min}/(body mass $\times$ length^2). We statistically compared measures of cross-sectional geometry between WT and KO mice using Welch's two-sample *t*-tests in R. We adjusted *P*-values for multiple comparisons using the Bonferroni correction.

Lean mass

To assess lean mass, we used a second cohort of 3-month-old male WT (n = 11) and Panx3-null (n = 12) mice. Lean mass was measured using quantitative magnetic resonance (QMR) analysis using an echo magnetic resonance imaging mobile unit at the Avian Facility of Advanced Research at The University of Western Ontario (London, ON, Canada). Each mouse was measured twice and the average of the two trials was used for statistical comparison. We compared body weight, lean mass and lean mass normalized by body weight between WT and KO mice using Welch's two-sample t-tests in R.

Results

Shape differences: KO mice demonstrate shorter femoral and humeral diaphyses and proportionally larger areas of bone at sites of muscle attachment when compared to WT mice

The allometric component of shape variation comprises 20 and 30% of the total shape variation for the femur and humerus, respectively. Both of these regressions were statistically significant ($P < 0.01$). PCA analyses for Procrustes data that include the allometric component of shape indicate that the majority of shape variation is within the first three principal components (PCs). Within the femur, PC1 accounts for 40% of the total variance, PC2 accounts for 16% of the variance, and PC3 accounts for 10% of the variance. For the humerus, 57% of the total variance is represented by PC1, 10% by PC2, and 7% by PC3. A bi-plot of the first two PCs for the femur (Fig. 2A) and humerus (Fig. 2B) shows that WT and KO mouse limb shape is differentiated along PC1, particularly in the humerus. Conversely, the two groups are overlapping along PC2. As PC1 in unscaled datasets represents the allometric component of shape, WT and KO mouse femoral and humeral morphology is differentiated by changes in growth.

Femoral shape and humeral shape variation after removal of the allometric component are also represented as bi-plots of the first two PCs (Fig. 2C,D). In the femur, PC1 accounts for 30% of the total variance, PC2 for 18% and PC3 for 11%. For the humerus, 40% of the total variance is represented by PC1, 15% by PC2, and 10% by PC3. When we remove the allometric component of shape there is no distinct separation of the groups. These groupings demonstrate that differences between WT and KO femoral and humeral shape are largely attributable to differences in allometric growth.

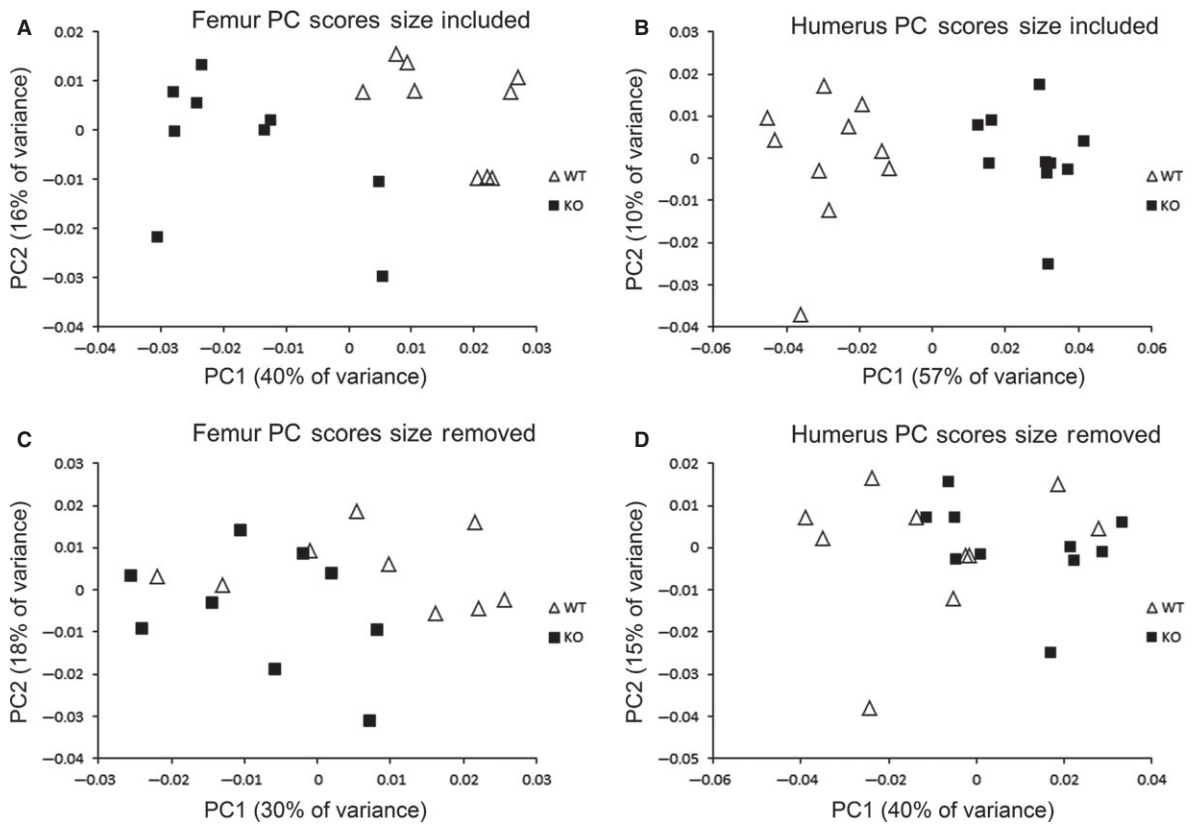

Fig. 2 Bi-plots of the first two principal components (PCs) for the femur and humerus. (A,B) include allometric component of shape and (C,D) exclude the allometric component of shape variation. Wildtype (WT) mice are represented by open triangles and knockout (KO) mice by closed squares. WT and KO humeral and femoral shape are differentiated along PC1 when the allometric component of shape is included (A,B).

EDMA FORM analysis of the femur reveals that approximately half (51%) of the inter-landmark linear distances differ significantly between WT and KO mice. The vast majority (49%) of the significantly different distances are greater in WT than in KO mice. All of the distances that are significantly greater in WT mice involve measures of diaphyseal length. Only one distance is significantly larger in KO mice and this distance is within the distal epiphysis (Fig. 3A–C). EDMA FORM analysis of the humerus reveals similar results. Again, 51% of the humeral inter-landmark distances differ significantly between WT and KO mice. All of these significantly different distances are greater in WT than in KO mice and all involve the length of the diaphysis (Fig. 3D–F).

EDMA SHAPE analysis of the femur reveals that over half of the linear inter-landmark distances (56%) are significantly different between WT and KO mice. Of these significantly different distances, 74% are larger in WT than in KO and 25% are greater in KO than in WT (Fig. 4A–C). EDMA SHAPE analysis of the humerus reveals that 71% of the inter-landmark distances differ significantly between WT and KO mice. Of these significantly different distances, 53% are larger in WT than in KO and 47% are larger in KO than in WT mice (Fig. 4D–G). In both bones, those distances that are significantly greater in KO than in WT mice involve large bony prominences for muscle attachment and/or the metaphyses/epiphyses of the bones. In SHAPE analysis, as in FORM analysis, the distances that are greater in WT than in KO are all measures of diaphyseal length.

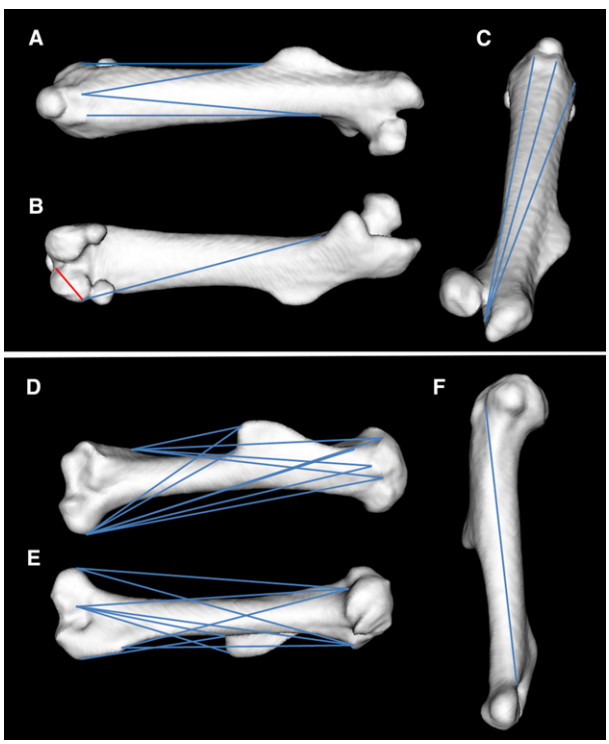

Fig. 3 Linear distances that are significantly different in FORM in the femur (A–C) and humerus (D–F) using confidence interval testing ($\alpha = 0.10$). Depicted are linear distances that differ between groups by $\geq 5\%$. Linear distances that are significantly greater in WT than KO mice are shown in blue and the distance that is greater in KO than WT mice is shown in red. These results indicate that WT mice have longer femoral and humeral diaphyses compared with KO mice. Views depicted for the femur: (A) rostral, (B) caudal and (C) supero-rostral. Views depicted for the humerus: (D) rostro-medial, (E) caudal and (F) supero-medial. The humerus and femur depicted are WT references.

Bone mineral density does not differ between KO and WT mice

We found no difference in bone mineral density of femora and humeri between KO and WT mice. For the femora, the average BMD for WT mice is 14.75 mg cm^{-3} ($\pm$ 2.81 SD) and is 16.77 mg cm^{-3} ($\pm$ 3.54 SD) for KO mice. For the humeri, the mean BMD for WT mice is 14.76 mg cm^{-3} ($\pm$ 2.41 SD) and is 15.41 mg cm^{-3} ($\pm$ 2.13 SD) for KO mice. These differences are not statistically significant ($P = 0.17$ femora; $P = 0.53$ humeri) as determined by Welch's two-sample *t*-tests.

Cross-sectional geometric properties analyses reveal that femora and humeri are more robust in KO mice than WT mice

Given that long bone cross-sectional properties are influenced by body mass, we compared weight between WT and KO mice. At the time of scanning, the average weight of WT mice was 26.3 g ($\pm$ 2.97 SD) and the average weight of KO mice was 24.6 g ($\pm$ 1.58 SD). There was no statistically significant difference in weight between the two groups ($P = 0.14$) as determined by Welch's two-sample *t*-test.

We compared cross-sectional properties of femora and humeri between WT and KO mice and summarize results in Table 2 and Figs 5 and 6. After correction for multiple tests using the Bonferroni correction, we found that KO mice have significantly larger measures of polar second moment of area (*J*) for both the femur and humerus, and for cortical area (CA) in the femur than WT mice. Using this conservative measure of significance, CA is not significantly different in the humerus, although the trend of greater CA in KO than in WT mice remains. Thus, KO mouse femora and humeri are predicted to have greater resistance to torsion (*J*) and compression (CA). Although KO mice have greater cortical area (CA), the proportion of cortical area to the whole section, as described by percent cortical area (%CA), is not significantly different between the groups. Additionally, the shape of the cortical cross-section that describes the distribution of cortical bone (I_{max}/I_{min}) is not significantly different between the groups. Our results indicate that KO femora and humeri are thicker than WT, but that the proportion and distribution of cortical bone are similar between groups.

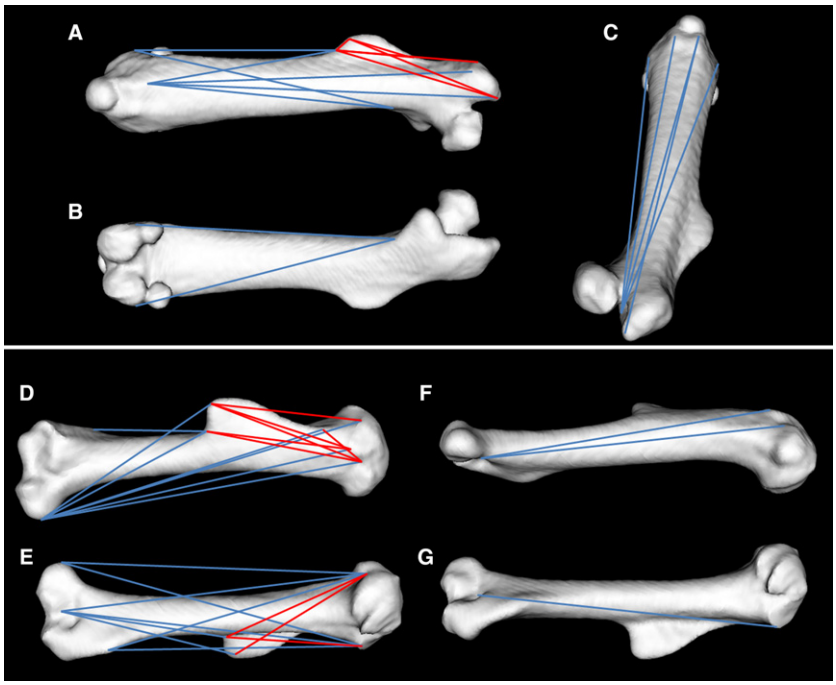

Fig. 4 Linear distances that are significantly different in SHAPE in the femur (A–C) and humerus (D–G) using ($\alpha = 0.10$). Depicted are linear distances that differ between groups by ≥5%. Linear distances that are significantly greater in WT than KO mice are shown in blue and the distances that are greater in KO than WT mice are shown in red. These results indicate that when the allometric component of shape is removed, WT mice have relatively longer humeral and femoral diaphyses compared with KO mice, and KO mice have proportionately larger muscle attachment sites for the femur and humerus compared with WT mice. Views depicted for the femur: (A) rostral, (B) caudal and (C) supero-rostral. Views depicted for the humerus: (D) rostro-medial, (E) caudal, (F) medial and (G) caudo-lateral. The humerus and femur depicted are WT references.

Lean mass and body weight do not differ between KO and WT mice

Our QMR analysis revealed no statistically significant differences in lean mass between WT and KO mice (Fig. 7A). As with our original mouse sample, there is no significant difference in body weight at 3 months between KO and WT mice (Fig. 7B). After standardizing lean mass by body weight, we still found no significant differences in lean mass between mouse groups (Fig. 7C).

Discussion

The *in vivo* effects of Panx3 on the skeletal system are just beginning to be uncovered. To date, there are only two studies that have employed Panx3-null mouse models, that of Moon et al. (2015), which includes many of the authors of the present study, and that of Oh et al. (2015). Our initial study using a global Panx3-null mouse was focused on the role of Panx3 in the onset of osteoarthritis (Moon et al. 2015). In that study, we found Panx3 ablation did not produce overt effects on skeletal development, but mice lacking Panx3, specifically in cartilage, were more resistant to developing osteoarthritis than WT mice following destabilization surgery of the medial meniscus (Moon et al. 2015). From these results, we suggested that Panx3 could be a potential therapeutic target for osteoarthritis. Oh et al. (2015) used a different global Panx3-null mouse to study the effects of Panx3 on skeletal development, as compared with previously published *in vitro* studies (i.e. Iwamoto et al. 2010; Ishikawa et al. 2011, 2014). Their results support the premise that Panx3 ablation results in prolonged chondrocyte proliferation, delays hypertrophic chondrocyte and osteoblast differentiation, and increases in intracellular cAMP levels. It was intriguing that the skeletal phenotype in the Oh et al. mouse was more severe than that found in our Panx3-null mouse but this may reflect variances in the cre-mediated recombination mouse used in each case as well as some possible subtle differences in the mouse strains used. Nevertheless, both studies point to a role for Panx3 in skeletal development and disease.

Here, we provide detailed insight into the *in vivo* effects of Panx3 on long bone phenotype through five novel findings: (1) Panx3 KO mice are absolutely smaller than WT mice, with the most significant differences in size localized to measures of diaphyseal length; (2) After scaling for size, Panx3 KO mouse femora and humeri have larger areas of muscle attachment compared with WT mice; (3) there are no significant differences in femoral or humeral BMD between Panx3 KO and WT mice; (4) Panx3 KO mice have significantly greater measures of femoral and humeral cross-sectional properties than WT mice; (5) body weight, lean mass, and lean mass standardized for body weight are not significantly different between Panx3 KO and WT mice. Our studies reported here are robust using sufficient mouse numbers to perform a rigorous statistical assessment of the effects of ablating Panx3 on the phenotype of both the femur and humerus.

Given the role that Panx3 has been proposed to play in the growth plate, it is not surprising that WT mice have longer diaphyses than Panx3 KO mice. Panx3 is expressed in pre-hypertrophic and hypertrophic chondrocytes in the developing growth plate (Iwamoto et al. 2010; Bond et al. 2011; Ishikawa et al. 2011). It appears to have a role in

Table 2 Summary of standardized cross-sectional properties of the femur and humerus and results from Welch's two-sample *t*-tests. Statistically significant differences between mouse groups after Bonferroni correction are in bold and indicated by an asterisk.

	Summary statistics							
	WT			KO			Welch's *t*-test	
Cross-sectional property	*n*	Mean	SD	*n*	Mean	SD	*t* score	*P*-value
Femur *J*	8	**0.13**	0.016	8	**0.19**	0.026	5.72	**0.00010***
Femur CA	8	**56.91**	3.71	8	**70.53**	5.88	5.54	**0.00012***
Femur %CA	8	66.76	1.8	8	69.17	4.33	1.45	0.18
Femur I_{max}/I_{min}	8	1.97	0.13	8	2.00	0.20	0.26	0.80
Humerus *J*	8	**0.049**	0.005	8	**0.060**	0.007	3.78	**0.002***
Humerus CA	8	33.01	2.68	8	36.43	2.57	2.60	0.021
Humerus %CA	8	83.15	1.49	8	83.16	2.15	0.014	0.99
Humerus I_{max}/I_{min}	8	1.41	0.1	8	1.36	0.09	0.97	0.35

CA, cortical area; %CA, percent cortical area; I_{max}, maximum second moment of area; I_{max}/I_{min}, diaphyseal shape; I_{min}, minimum second moment of area; *J*, polar second moment of area; KO knockout mice; *n*, number of mice; SD, standard deviation; WT, wildtype mice.

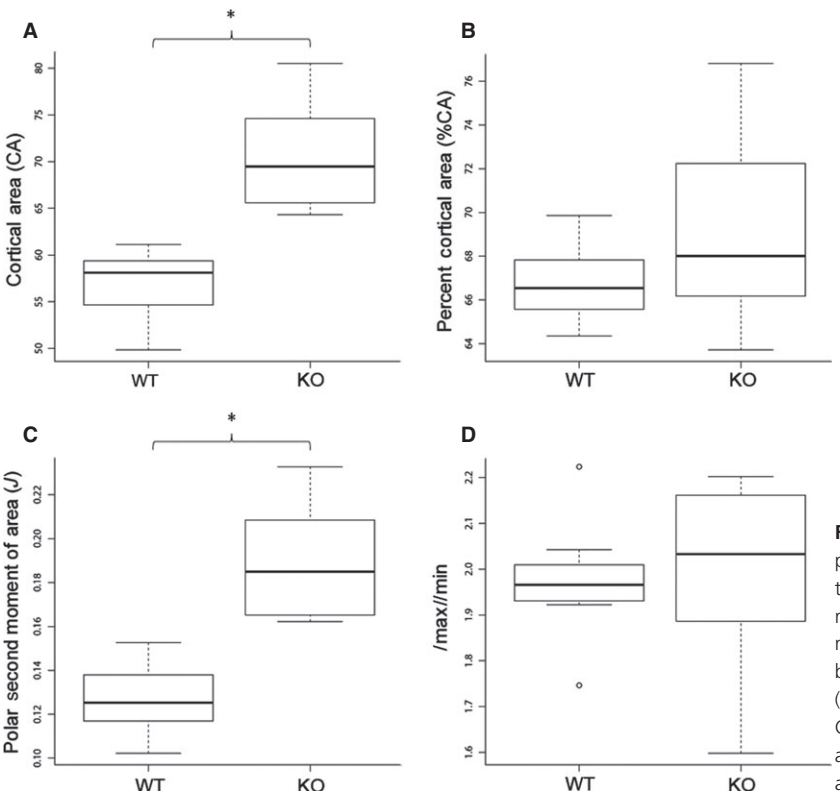

Fig. 5 (A) Femur cortical area (CA). (B) Femur percent cortical area (%CA = cortical area/total subperiosteal area × 100). (C) Femur midshaft torsional rigidity (*J*). (D) Femur midshaft shape (I_{max}/I_{min}). All values have been standardized by body size. Knockout (KO) mice have statistically larger measures of CA and *J* compared with wildtype (WT) mice as determined by Welch's two-sample *t*-tests after Bonferroni correction ($p < 0.0125$).

regulating growth at the growth plate by inhibiting chondrocyte proliferation and initiating chondrocyte differentiation (Iwamoto et al. 2010; Oh et al. 2015). Mature (differentiated) chondrocytes secrete the matrix that calcifies and forms the framework for ossification by osteoblasts and osteocytes, thereby increasing bone length (Kronenberg, 2003; Ross & Pawlina, 2011). Whereas longitudinal bone growth requires chondrocyte hypertrophy, ossification depends on osteoblast and osteocyte differentiation. Panx3 is thought to positively regulate differentiation of osteoprogenitor cells into osteoblasts (Ishikawa et al. 2014). Thus, growth in bone length requires that chondrocytes in the growth plate mature and differentiate, and that osteoblasts are available for ossification. We suggest that the

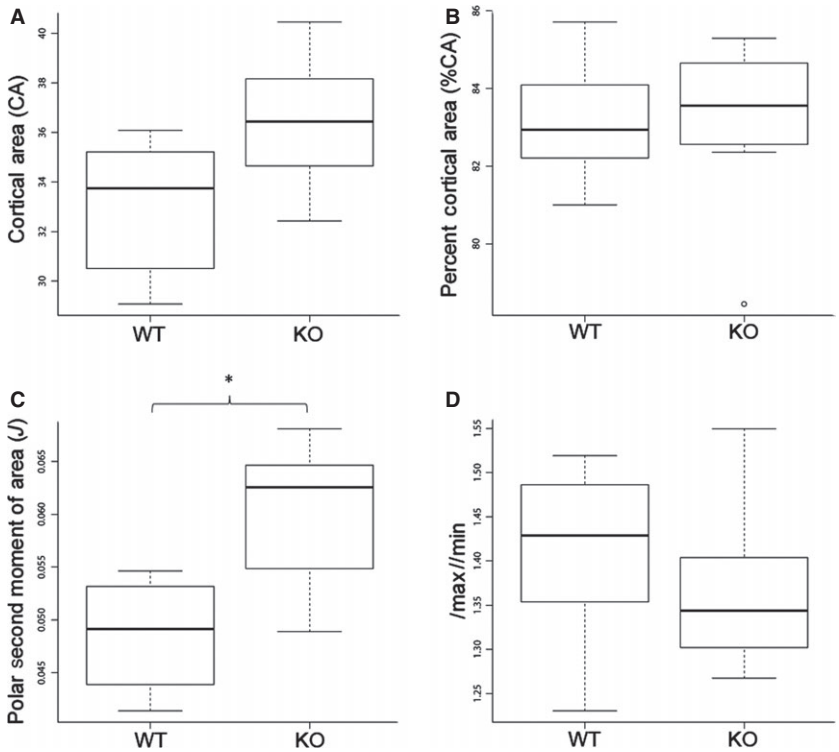

Fig. 6 (A) Humerus cortical area (CA). (B) Humerus percent cortical area (% CA = cortical area/total subperiosteal area × 100). (C) Humerus midshaft torsional rigidity (*J*). (D) Humerus midshaft shape (I_{max}/I_{min}). All values have been standardized by body size. Knockout (KO) mice have statistically larger measures of *J* compared with wildtype (WT) mice as determined by Welch's two-sample *t*-tests after Bonferroni correction ($p < 0.0125$).

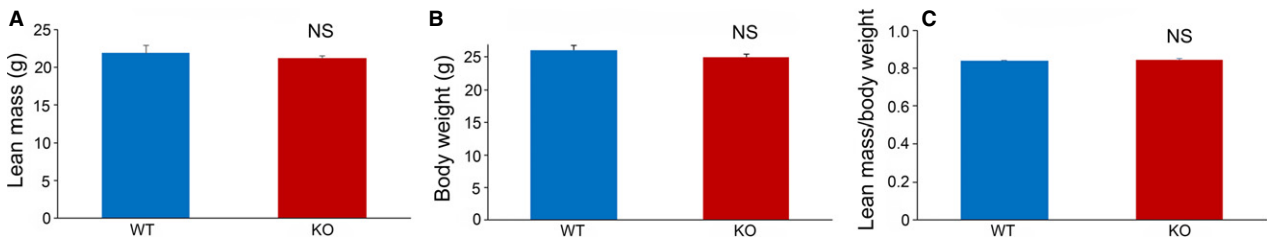

Fig. 7 Quantitative magnetic resonance analysis measures for whole body lean mass (A), whole body weight (B), and whole body lean mass normalized by whole body weight (C). Comparisons between wildtype (WT) and Panx3 knockout (KO) mice for all three measures are not statistically significant (ns) as determined by Welch's two-sample *t*-tests.

reduced femoral and humeral diaphyseal length found in our Panx3 KO mice is due to a reduction of hypertrophic chondrocytes and osteoblasts in the growth plate.

When we remove the allometric component of shape, there are no differences in overall femur and humerus morphology between KO and WT mice. However, we can still detect important localized shape differences. Wildtype mice have proportionately longer femoral and humeral diaphyses than KO mice. Given the role of Panx3 in the developing growth plate of long bones, we expected this proportional shape change. Interestingly, there were also many distances that were relatively larger in KO mice than WT mice. These distances clustered in areas of muscle attachment sites; specifically the third trochanter of the femur and the deltoid tuberosity of the humerus.

Results from our cross-sectional geometric analyses show that KO mice have significantly larger measures of second polar moment of area (*J*) for both the femur and humerus, and larger measures of femoral cortical area (CA) compared with WT mice. As *J* is a predictor of torsional rigidity, our results suggest that both the femur and humerus in KO mice are more resistant to deformation under torsional loads than are WT mice (Ruff & Hayes, 1983). Similarly, CA is a predictor of resistance to axial compressive loads and is largely affected by body mass (Ruff & Hayes, 1983); thus, femora of KO mice can likely withstand greater compressive loads than WT mice can. Although Panx3 KO mice have more robust bones in cross-section than WT mice, differences in cross-sectional properties are isotropic; that is, KO long bone cross-sections are a scaled-up version of WT long bones.

Cross-sectional geometric properties are often used to compare the load history of bones (Ruff & Hayes, 1983; Shaw & Stock, 2009a,b). Changes in cross-sectional

properties are usually interpreted as due to differences in body mass, intensity or pattern of activity, and/or muscle mass (Nunamaker et al. 1990; Carlson & Judex, 2007; Shaw & Stock, 2009a,b). The WT and KO mice used in this study have the same body mass (both cohorts), and while not specifically studied, the two groups did not display overt differences in activity patterns or intensity. Additionally, KO mice have proportionately increased areas of muscle attachment on both the femur and humerus compared with WT mice. It is possible that the cross-sectional differences and more subtle shape changes between mouse groups are due to differences in muscle–bone interactions. Indeed, Panx3 has been found expressed in mouse skeletal muscle and this expression is modulated during myoblast differentiation (Langlois et al. 2014). However, we conducted QMR analysis on a separate cohort of 3-month-old male Panx3 KO and WT mice and found no significant difference in lean body mass. While this measure of lean mass includes muscle tissue throughout the body and organ tissue, the lack of difference suggests that Panx3 does not have a strong effect on muscle mass, though it may affect other skeletal muscle properties that are beyond the current study.

In summary, it appears that Panx3 may function as a regulator of bone growth and development. Our results uncover patterns of phenotypic change in Panx3 KO mice that may indicate a dual role for Panx3 in long bone growth and development. The greatest effect found in our mice is in long bone length, where WT mice have longer femoral and humeral diaphyses than KO mice. Long bone length is determined by growth plate activity and thus Panx3 may function as a positive regulator of bone growth at the growth plate. We also found that KO mice had larger areas of muscle attachment and greater measures of mid-shaft cross-sectional properties. Changes to muscle attachment sites and to cortical bone in cross-section are largely influenced by functional demands postnatally, and are therefore more strongly affected by processes of remodeling than initial developmental processes. Given our findings, we suggest that Panx3 may play an inhibitory role in bone remodeling.

Acknowledgements

We thank Drs Joseph Umoh and David Holdsworth of the Preclinical Imaging Research Centre at Robarts Research Institute (London, ON, Canada) for their assistance with mouse scanning and measurement of BMD. This study was funded by a Canadian Institutes of Health Research operating grant (MOP130530) to D.W.L., F.B. and S.P. D.W.L. and F.B. are supported by Canada Research Chair Awards.

References

Baab KL, McNulty KP, Rohlf FJ (2012) The shape of human evolution: a geometric morphometrics perspective. *Evol Anthropol* **21**, 151–165.

Bao L, Locovei S, Dahl G (2004) Pannexin membrane channels are mechanosensitive conduits for ATP. *FEBS Lett* **572**, 65–68.

Baranova A, Ivanov D, Petrash N, et al. (2004) The mammalian pannexin family is homologous to the invertebrate innexin gap junction proteins. *Genomics* **83**, 706–716.

Beaucage KL, Xiao A, Pollmann SI, et al. (2014) Loss of P2X7 nucleotide receptor function leads to abnormal fat distribution in mice. *Purinergic Signal* **10**, 291–304.

Bond SR, Naus CC (2014) The pannexins: past and present. *Front Physiol* **5**, 58.

Bond SR, Lau A, Penuela S, et al. (2011) Pannexin 3 is a novel target for Runx2, expressed by osteoblasts and mature growth plate chondrocytes. *J Bone Miner Res* **26**, 2911–2922.

Bookstein FL (1991) *Morphometric Tools for Landmark Data: Geometry and Biology*. New York: Cambridge University Press.

Carlson KJ, Judex S (2007) Increased non-linear locomotion alters diaphyseal bone shape. *J Exp Biol* **210**, 3117–3125.

Frelat MA, Katina S, Weber GW, et al. (2012) Technical note: a novel geometric morphometric approach to the study of long bone shape variation. *Am J Phys Anthropol* **149**, 628–638.

Gower J (1975) Generalized Procrustes analysis. *Psychometrika* **40**, 33–51.

Granton PV, Norley CJ, Umoh J, et al. (2010) Rapid in vivo whole body composition of rats using cone beam μCT. *J Appl Physiol*, **109**, 1162–1169.

Hammond CL, Schulte-Merker S (2009) Two populations of endochondral osteoblasts with differential sensitivity to Hedgehog signalling. *Development* **136**, 3991–4000.

Ishikawa M, Iwamoto T, Nakamura T, et al. (2011) Pannexin 3 functions as an ER Ca^{2+} channel, hemichannel, and gap junction to promote osteoblast differentiation. *J Cell Biol* **193**, 1257–1274.

Ishikawa M, Iwamoto T, Fukumoto S, et al. (2014) Pannexin 3 inhibits proliferation of osteoprogenitor cells by regulating Wnt and p21 signaling. *J Biol Chem* **289**, 2839–2851.

Iwamoto T, Nakamura T, Doyle A, et al. (2010) Pannexin 3 regulates intracellular ATP/cAMP levels and promotes chondrocyte differentiation. *J Biol Chem* **285**, 18948–18958.

Klingenberg CP (2011) MorphoJ: an integrated software package for geometric morphometrics. *Mol Ecol Resour* **11**, 353–357.

Kronenberg HM (2003) Developmental regulation of the growth plate. *Nature* **423**, 332–336.

Langlois S, Xiang X, Young K, et al. (2014) Pannexin 1 and pannexin 3 channels regulate skeletal muscle myoblast proliferation and differentiation. *J Biol Chem* **289**, 30717–30731.

Le Vasseur M, Lelowski J, Bechberger JF, et al. (2014) Pannexin 2 protein expression is not restricted to the CNS. *Front Cell Neurosci* **8**, 1–13.

Lele S, Richtsmeier JT (1991) Euclidean distance matrix analysis: a coordinate-free approach for comparing biological shapes using landmark data. *Am J Phys Anthropol* **86**, 415–427.

Lele S, Richtsmeier JT (2001) *An Invariant Approach to Statistical Analysis of Shapes*. New York: Chapman & Hall.

Long F, Ornitz DM (2013) Development of the endochondral skeleton. *Cold Spring Harb Perspect Biol* **5**, a008334.

Moon PM, Penuela S, Barr K, et al. (2015) Deletion of Panx3 prevents the development of surgically induced osteoarthritis. *J Mol Med (Berl)* **93**, 845–856.

Nunamaker DM, Butterweck DM, Provost MT (1990) Fatigue fractures in thoroughbred racehorses: relationships with age, peak bone strain, and training. *J Orthop Res* **8**, 604–611.

Oh S-K, Shin J-O, Baek J-I, et al. (2015) Pannexin 3 is required for normal progression of skeletal development in vertebrates. *FASEB J* **29**, 4473–4484.

Panchin Y, Kelmanson I, Matz M, et al. (2000) A ubiquitous family of putative gap junction molecules. *Curr Biol* **10**, R473–R474.

Penuela S, Bhalla R, Gong XQ, et al. (2007) Pannexin 1 and pannexin 3 are glycoproteins that exhibit many distinct characteristics from the connexin family of gap junction proteins. *J Cell Sci* **120**, 3772–3783.

Penuela S, Celetti SJ, Bhalla R, et al. (2008) Diverse subcellular distribution profiles of pannexin 1 and pannexin 3. *Cell Commun Adhes* **15**, 133–142.

Penuela S, Gehi R, Laird DW (2013) The biochemistry and function of pannexin channels. *Biochim Biophys Acta* **1828**, 15–22.

Penuela S, Harland L, Simek J, et al. (2014) Pannexin channels and their links to human disease. *Biochem J* **461**, 371–381.

Pest MA, Beier F (2014) Is there such a thing as a cartilage-specific knockout mouse? *Nat Rev Rheumatol* **10**, 702–704.

Porto A, Shirai LT, de Oliveira FB, et al. (2013) Size variation, growth strategies, and the evolution of modularity in the mammalian skull. *Evolution* **67**, 3305–3322.

Rohlf FJ, Slice DE (1990) Extensions of the Procrustes method for optimal superimposition of landmarks. *Syst Zool* **39**, 40–59.

Ross M, Pawlina W (2011) *Histology: A Text and Atlas: with Correlated Cell and Molecular Biology*. Philadelphia: Wolters Kluwer/Lippincott Williams and Wilkins Health.

Ruff CB (2008) Biomechanical analyses of archaeological human skeletal samples. In: *Biological Anthropology of the Human Skeleton* (eds Katzenberg MA, Saunders SR), pp. 183–206. New York: John Wiley & Sons.

Ruff CB, Hayes WC (1983) Cross-sectional geometry of pecos pueblo femora and tibiae – a biomechanical investigation. 1. Method and general patterns of variation. *Am J Phys Anthropol* **60**, 359–381.

Scemes E, Spray DC, Meda P (2009) Connexins, pannexins, innexins: novel roles of 'hemi-channels'. *Pflugers Arch* **457**, 1207–1226.

Shaw CN, Stock JT (2009a) Habitual throwing and swimming correspond with upper limb diaphyseal strength and shape in modern human athletes. *Am J Phys Anthropol* **140**, 160–172.

Shaw CN, Stock JT (2009b) Intensity, repetitiveness, and directionality of habitual adolescent mobility patterns influence the tibial diaphysis morphology of athletes. *Am J Phys Anthropol* **140**, 149–159.

Sosinsky GE, Boassa D, Dermietzel R, et al. (2011) Pannexin channels are not gap junction hemichannels. *Channels (Austin)* **5**, 193–197.

Tsang KY, Chan D, Cheah KS (2015) Fate of growth plate hypertrophic chondrocytes: death or lineage extension? *Dev Growth Differ* **57**, 179–192.

Turmel P, Dufresne J, Hermo L, et al. (2011) Characterization of pannexin1 and pannexin3 and their regulation by androgens in the male reproductive tract of the adult rat. *Mol Reprod Dev* **78**, 124–138.

Wang XH, Streeter M, Liu YP, et al. (2009) Identification and characterization of pannexin expression in the mammalian cochlea. *J Comp Neurol* **512**, 336–346.

White A, Wallis G (2001) Endochondral ossification: a delicate balance between growth and mineralisation. *Curr Biol* **11**, R589–R591.